J Neurophysiol 97: 901–911, 2007.
First published November 8, 2006; doi:10.1152/jn.00974.2006.

Morphological and Electrophysiological Properties of GABAergic and Non-GABAergic Cells in the Deep Cerebellar Nuclei

Marylka Uusisaari,[1] Kunihiko Obata,[2] and Thomas Knöpfel[1]

[1]*Laboratory for Neuronal Circuit Dynamics and* [2]*Obata Research Unit, Brain Science Institute, The Institute of Physical and Chemical Research, Wako City, Saitama, Japan*

Submitted 12 September 2006; accepted in final form 3 November 2006

Uusisaari M, Obata K, Knöpfel T. Morphological and electrophysiological properties of GABAergic and non-GABAergic cells in the deep cerebellar nuclei. *J Neurophysiol* 97: 901–911, 2007. First published November 8, 2006; doi:10.1152/jn.00974.2006. The deep cerebellar nuclei (DCN) integrate inputs from the brain stem, the inferior olive, and the spinal cord with Purkinje cell output from cerebellar cortex and provide the major output of the cerebellum. Despite their crucial function in motor control and learning, the various populations of neurons in the DCN are poorly defined and characterized. Importantly, differences in electrophysiological properties between glutamatergic and GABAergic cells of the DCN have been largely elusive. Here, we used glutamate decarboxylase (GAD) 67-green fluorescent protein (GFP) knock-in mice to unambiguously identify GABAergic (GAD-positive) and non-GABAergic (GAD-negative, most likely glutamatergic) neurons of the DCN. Morphological analysis of DCN neurons patch-clamped with biocytin-containing electrodes revealed a significant overlap in the distributions of the soma sizes of GAD-positive and GAD-negative cells. Compared with GAD-negative DCN neurons, GAD-positive DCN neurons fire broader action potentials, display stronger frequency accommodation, and do not reach as high firing frequencies during depolarizing current injections. Furthermore, GAD-positive cells display slower spontaneous firing rates and have a more shallow frequency-to-current relationship than the GAD-negative cells but exhibit a longer-lasting rebound depolarization and associated spiking after a transient hyperpolarization. In contrast to the rather homogeneous population of GAD-positive cells, the GAD-negative cells were found to consist of two distinct populations as defined by cell size and electrophysiological features. We conclude that GABAergic DCN neurons are specialized to convey phasic spike rate information, whereas tonic spike rate is more faithfully relayed by the large non-GABAergic cells.

INTRODUCTION

The deep cerebellar nuclei (DCN) are in a key position within the cerebellar circuitry. Neurons of the DCN receive synaptic inputs from all cerebellar afferents, are the main target of Purkinje cells, and their own axons provide the major output of the cerebellum.

DCN neurons were originally classified on the basis of cell morphological criteria by Chan-Palay (1977) into at least six distinct types. A more pragmatic classification based on connectivity and transmitter content differentiates large and small projection neurons and local circuit neurons (Chen and Hillman 1993; Fredette and Mugnaini 1991). Within this classification, GABAergic neurons are thought to represent small local circuit neurons (that also contain glycine; Chen and Hillman 1993) and projection neurons targeting the inferior olive (IO), whereas glutamatergic neurons are equivalent to the large neurons projecting to red nucleus and other precerebellar sites. A single Purkinje cell can innervate both glutamatergic and GABAergic cells (De Zeeuw and Berrebi 1995; Teune et al. 1998) and thus can have both an inhibiting and a disinhibiting effect on DCN output neurons. Disinhibition and differences in action potential (AP) firing dynamics (e.g., in firing frequency adaptation) increase the complexity of the DCN circuit dynamics beyond the level that is considered in most present cerebellar network models (Lisberger and Sejnowski 1992; Medina et al. 2001; Silberberg et al. 2005). Electrophysiological studies of DCN neurons published to date either did not specify the cell type recorded or referred to large neurons, often presumed glutamatergic, because they are more likely sampled with extracellular or intracellular recording techniques. The properties of these large but unidentified DCN neurons were described in classical and more recent work (Afshari et al. 2004; Aizenman and Linden 1999; Czubayko et al. 2001; Llinas and Muhlethaler 1988; Molineux et al. 2006; Muri and Knöpfel 1994; Raman et al. 2000; Sultan et al. 2003).

It is not clear how these electrophysiological characteristics correlate with morphologically and biochemically defined cell types. Previous studies did not reveal strong correlations between morphological characteristics and electrophysiological properties (Aizenman et al. 2003; Czubayko et al. 2001). However, these studies did not directly attempt to differentiate glutamatergic and GABAergic neurons. A concurrent study by Molineux and colleagues (2006) found correlation between the expression of Ca_v3 subtypes and the bursting propensity; however, even though the "weak-bursting" phenotype was restricted to non-GABAergic (GAD67-negative) cells, both GAD67-positive and GAD67-negative cells could express a "bursting" phenotype. Thus the bursting phenotype only weakly correlated with the transmitter used by DCN neurons.

To address the issue of identification and characterization of GABAergic versus non-GABAergic (presumed glutamatergic) cells in the DCN, we used glutamate decarboxylase 67-green fluorescent protein (GFP) knock-in mice to record from identified GABAergic (GAD-positive, GAD+) and non-GABAergic (GAD-negative, GAD−) neurons in DCN slice preparation. We characterized the active and passive membrane properties of GAD+ and GAD− neurons and correlated electrophysiological measures with morphometric data obtained with biocytin histochemistry. We found that the GAD+ and GAD− cells exhibit similar morphological features with

Address for reprint requests and other correspondence: T. Knöpfel, Laboratory for Neuronal Circuit Dynamics, Brain Science Institute, RIKEN, 2-1 Hirosawa, Wako-shi, Saitama, 351-0198, Japan (E-mail: tknopfel@brain.riken.jp).

The costs of publication of this article were defrayed in part by the payment of page charges. The article must therefore be hereby marked "*advertisement*" in accordance with 18 U.S.C. Section 1734 solely to indicate this fact.

significant differences revealed only when comparing population averages. Electrophysiological features were more distinct and a combination of electrophysiological measures was found to be necessary and sufficient for reliable determination of cell identity (GABAergic vs. non-GABAergic).

METHODS

Generation of knock-in animals (GAD67-GFP)

The generation of GAD67-GFP knock-in mice was previously described elsewhere (Tamamaki et al. 2003). In brief, a cDNA-encoding enhanced GFP (EGFP; ClonTech, Palo Alto, CA) was targeted to the locus encoding GAD67 using homologous recombination. We used heterozygotous GAD67-GFP knock-in mice identified by PCR of tail DNA (Tamamaki et al. 2003). Experimental protocols were approved by the RIKEN Experimental Animal Committee and conducted in compliance with the Guidelines for the Use of Animals in Neuroscience Research (The Society for Neuroscience, Washington, DC).

Slice preparation

Young (postnatal days 14–20) mice were anesthetized with halothane and decapitated. The cerebellum was quickly removed and mounted for sectioning with a vibratome (Leica VT1000S, Leica Microsystems, Nussloch, Germany) using ceramic blades (Campden Instruments, Loughborough, UK) in ice-cold standard physiological solution [artificial cerebrospinal fluid (ACSF)] containing (in mM): NaCl, 124; KCl, 3; KH_2PO_4, 1.2; $MgSO_4$, 1.9; glucose, 20; $NaHCO_3$, 26; and $CaCl_2$, 2, and gassed with 95% O_2-5% CO_2. The two to three coronal slices (300 μm) containing the DCN were allowed to recover for >1 h in oxygenated ACSF at room temperature (21–23°C) and used for recording during the next 4 h.

Electrophysiological recordings

Slices were transferred to a submerged-type chamber mounted on a Leica DMLFSA microscope equipped with differential interference contrast (DIC) optics, whole field epifluorescence (Till Photonics, Gräfelfing, Germany), and laser scanning confocal (Leica TCS SP2; Leica Microsystems, Mannheim, Germany) imaging. Slices were superfused with gassed ACSF (2–3 ml/min, at 23–24°C). In some experiments recording temperature was switched from 25 to 35°C by means of an inline solution heater (Warner Instruments, Hamden, CT). Borosilicate glass–patch electrodes (2-mm OD, 4–7 MΩ) were filled with intracellular solution containing (in mM) K-gluconate, 140; NaCl, 10; HEPES, 10; EGTA, 0.2; Mg-ATP, 4; Na-GTP, 0.4; glutathione, 5; and biocytin, 8, pH adjusted to 7.3 with KOH (280 mOsm). Cell-attached voltage-clamp and whole cell patch-clamp recordings in current-clamp mode were acquired and controlled using the Axon 700B Multiclamp amplifier and pClamp acquisition software (Axon Instruments, Union City, CA). The sampling frequency was 10 kHz except in Fig. 8, where it was 100 kHz. No significant differences in measured and averaged action potential shapes were found. After breaking from a gigaohm seal into whole cell configuration, cells were kept subthreshold for spontaneous AP firing (usually −65 to −70 mV) by injection of up to −250-pA holding current.

In the beginning of each experiment, the input resistance and time constant were measured using hyperpolarizing current steps small enough so that the I_h-like voltage sag was not resolved, and from these values the apparent membrane capacitance (C_m) was estimated. All subsequent amplitudes of current steps were normalized on C_m, so that increments in current steps amounted to 0.3 pA/pF. The standard test protocols included series of 1-s hyperpolarizing and depolarizing current steps from the holding membrane potential of around −65 mV as well as prolonged (several minutes) recording of spontaneous firing under zero holding current.

In some cell-attached experiments 20 μM 6-nitro-7-sulfamoylbenzo(f)-quinoxaline-2,3-dione (NBQX, Tocris), 50 μM D-2-amino-5-phosphonopentoate (D-APV, Tocris), and 100 μM picrotoxin (PiTX; Sigma) were used to block synaptic transmission. Electrophysiological characterization was concluded within 5–10 min after breaking into whole cell mode but the whole cell configuration was kept for ≥20 min to ensure sufficient biocytin fill by diffusive loading through the patch pipette. The electrode was then gently withdrawn from the cell body. Slices were kept for an additional hour in room temperature ACSF to provide sufficient time for biocytin diffusion into distal dendrites and axons and then fixed in 4% paraformaldehyde in 0.1 M PBS (pH 8) at 4°C for 12 h.

Measurement of electrophysiological parameters

For analysis of the shape of evoked APs (eAPs), the first APs fired by each cell in response to a series of increasing depolarizing current steps were peak-aligned and averaged. For steady-state AP (ssAP) shape analysis, the same was performed for several tens of consecutive APs recorded under zero holding current condition. The half-width and peak amplitude of these average APs were measured and the grand average over APs of a given cell type were calculated. For frequency–current (*f–I*) measures, the mean firing frequency evoked with increasing current steps was measured; for frequency adaptation, the interspike intervals of APs evoked in response to a current step that evoked around 40-Hz firing were measured and normalized to peak values. I_h-type depolarizing sag in the voltage response to hyperpolarizing current injections was normalized to initial maximum hyperpolarization evoked by a −1.5-pA/pF current step. The strength of rebound depolarization (RD) after a 1-s-long, −1.5-pA/pF current step was quantified in terms of the duration of RD at half-amplitude.

Biocytin histochemistry

Fixed slices were washed with PBS and endogenous peroxidases were quenched by a 5-min incubation in 1% H_2O_2. Tissue was reacted overnight in avidin–biotin complex (ABC Elite kit; Vector Laboratories, Burlingame, CA) at 4°C. Finally, biocytin was demonstrated by 3,3′-diaminobenzidine tetrahydrochloride histochemistry.

Confocal imaging and anatomical quantification

For morphometry, slices with biocytin-stained cells were mounted on objective glass under coverslip and digitally imaged using a Leica DC500 digital camera on a Leica DMRE microscope.

Whole *z*-axis stack sequence of the biocytin-filled cells was projected into a single image using Image Pro Plus 5.1 software (Media Cybernetics, Silver Spring, MD) and the cell body area was calculated as the area of the cross section of the cell body in the image. Dendritic distance was measured as the longest distance between a visible dendrite tip and soma center. The branching index (BI) was determined by dividing the number of dendritic branches crossing a 30-μm-radius circle centered on the soma by the number of primary dendrites visible. All spatial features were analyzed using ImagePro Plus 5.1 software.

Confocal images of GFP-expressing fixed DCN slices were acquired using either the Olympus Fluoview Fv500 (Olympus, Tokyo, Japan; Fig. 1*A*) or Leica TCS SP2 confocal (Fig. 1*B*) microscope.

Data analysis

Electrophysiological data were analyzed using Clampfit 9.2 software (Axon Instruments).

Statistical analysis of all parameters was performed using OriginLab 7 software (OriginLab, Northampton, MA). Because no differ-

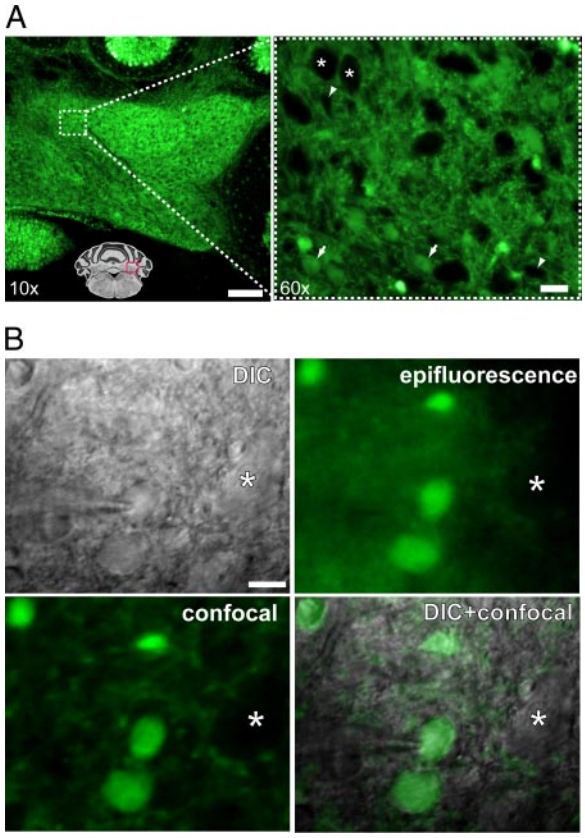

FIG. 1. Visualization of GABAergic neurons in the deep cerebellar nuclei (DCN). *A*: low- (*left*) and high-resolution (*right*) confocal images of a paraformaldehyde-fixed coronal cerebellar slice from a glutamate decarboxylase (GAD) 67-green fluorescent protein (GFP) knock-in mouse. Scale bars: 100 μm (*left*) and 20 μm (*right*). *Inset*: schematic of the approximate position (red rectangle) of imaged area; white rectangle indicates area shown at higher resolution on the *right*. Note large (white asterisks) and small (arrowheads) GFP-negative cells, and that some of the latter group are similar in size with larger GFP-positive cells (arrows). *B*: typical example of fluorescence-assisted selection of cells for patch-clamp recordings. Images from an acute slice in differential interference contrast (DIC, *top left*), whole-field epifluorescence (*top right*), and confocal fluorescence (*bottom left*) configuration. *Bottom right* image is a superimposition of DIC and confocal images. Note GABAergic terminals decorating the cell body of a large, non-GFP–expressing cell (asterisk). Scale bar: 20 μm.

ences over the studied age range were seen in the measured parameters, the data from all cells were pooled. All data are presented as means ± SE; for statistical significance, Student's *t*-test was used unless otherwise specified.

RESULTS

Identification of GABAergic cells in the DCN

The cells of DCN are a heterogeneous population of glutamatergic and GABAergic neurons (Chan-Palay 1977; Chen and Hillman 1993; De Zeeuw and Berrebi 1995; Fredette and Mugnaini 1991; Teune et al. 1998). GABAergic neurons can unambiguously be identified in "knock-in" mice that express GFP under the natural regulatory sequences for GAD67 (Tamamaki et al. 2003). As seen in confocal-scan images (Fig. 1*A*; paraformaldehyde-fixed section), the deep cerebellar nuclei of these mice contain a large population of brightly fluorescent neurons. Both the shapes of the DCN and the prominent projections from cerebellar cortex are easily seen. At larger magnification (Fig. 1*A*, *right*) individual cells are clearly visible. Notably, even though the largest cell bodies (marked with white asterisks) belong to non-GFP–expressing cells (i.e., GAD67-negative, GAD−), it was immediately evident that not all smaller cells were GFP-expressing (thus GAD67-positive, GAD+; compare cell bodies marked with arrowheads and arrows). Because of this, all of the recordings reported in this study were performed using slices from GFP knock-in mice for unambiguous identification of GABAergic neurons.

The GFP fluorescence of GAD+ cells was sufficiently bright as to perform targeted patch-clamp recordings using epifluorescence in combination with DIC microscopy (Fig. 1*B*).

Morphological properties of GAD− and GAD+ cells

Whole cell patch-clamp recordings were performed with biocytin-containing pipettes; 43 GAD− and 21 GAD+ biocytin-filled cells were recovered after fixing the slices (examples shown in Fig. 2, *A–D*) and their morphological features were analyzed. Consistent with earlier studies (Chan-Palay 1977) both GAD+ and GAD− cells exhibited a wide range of dendritic morphologies. Both cell groups included neurons with axons that either coursed locally or that projected to more distant targets (arrowheads in Fig. 2, *B* and *C*). Spines were occasionally seen on both GAD+ and GAD− cells (see *insets* in Fig. 2, *A* and *D*).

In general, GAD− neurons had larger cell bodies and a more complex dendritic morphology than those of GAD+ neurons. However, quantitative analysis revealed clearly overlapping distributions of several key morphometric measures (Fig. 3, *A–D*). On average, the GAD-negative cells were larger (average soma cross-sectional area 322 ± 20 μm^2; Fig. 3*A*), had more primary dendrites (PDs) (3.66 ± 0.16; Fig. 3*B*) that extended further away (174 ± 11 μm; Fig. 3*C*) from the soma

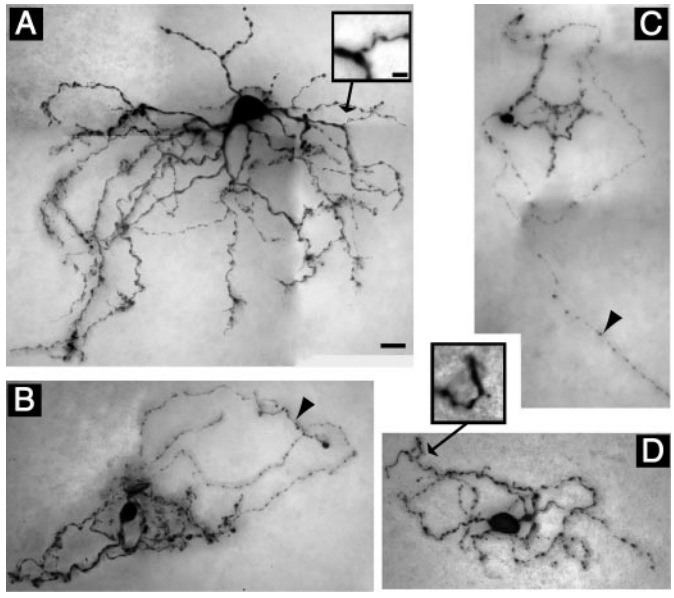

FIG. 2. Morphology of biocytin-filled DCN neurons. *A–D*: collages of *z*-stack projections of GFP-negative (GAD−; *A* and *B*) and GFP-positive cells (GAD+; *C* and *D*). *Insets* in *A* and *D* show larger magnification of spinelike structures. Arrowheads in *B* and *C* indicate axons. Scale bar in large images: 20 μm; *insets*: 5 μm.

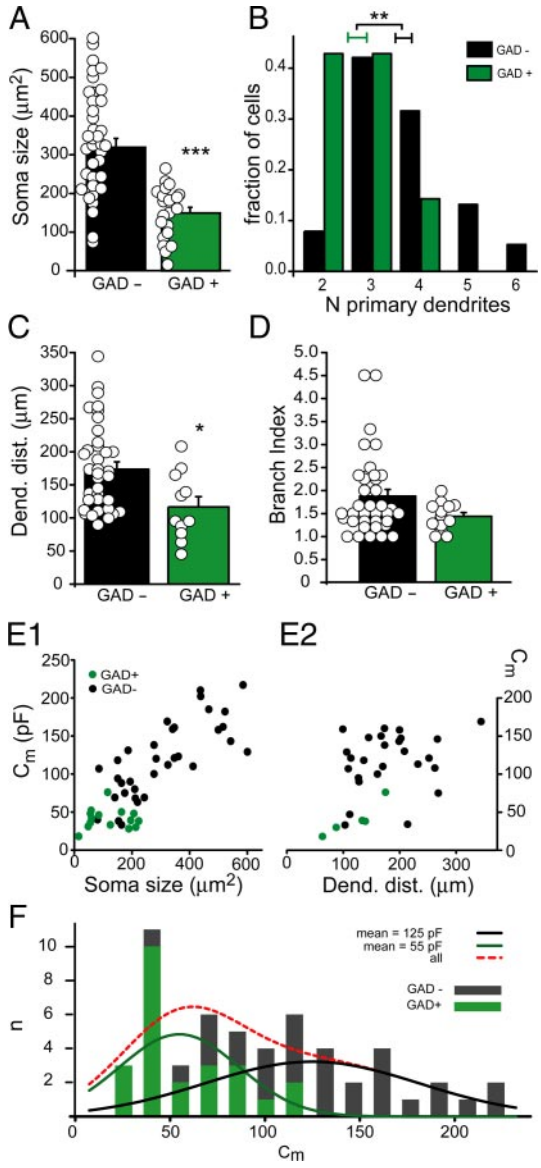

FIG. 3. Quantitative morphometry of biocytin-filled GAD− and GAD+ DCN neurons. Black and green colors are used throughout to highlight measures from GAD− and GAD+ neurons, respectively. *A*: size of cell bodies; mean ± SE values (bars) along with individual values (circles). *B*: distribution of the number of primary dendrites. Black, GAD− cells ($n = 38$); green, GAD+ cells ($n = 14$). Horizontal bars indicate mean ± SE values. *C* and *D*: maximal extension of dendritic processes and branch index (number of branches/primary dendrite crossing a 30-μm circle around soma center); mean ± SE values (bars) along with individual values (circles). *E*: scatterplot of individual membrane capacitances (C_m) vs. soma size (*E1*) and maximal dendritic distance (*E2*). Black and green dots correspond to values obtained from GAD− and GAD+ cells, respectively. *F*: distribution of pooled GAD− and GAD+ cell C_m values (15-pF bin size; GAD−, $n = 30$; GAD+, $n = 24$). Red line is dual Gaussian fit, constrained by the approximate mean C_m values of GAD− and GAD+ cells (125 and 55 pF, respectively). Black and green lines are the 2 Gaussian components of the fit. Asterisks denoting statistical significance: $*P < 0.05$; $**P < 0.01$; $***P < 0.001$.

than the GAD+ cells (area 150 ± 15 μm^2, $P < 0.0001$; 2.7 ± 0.26 PDs, $P < 0.01$; dendritic extension 117 ± 16 μm, $P < 0.05$). The GAD− and GAD+ cells did not differ significantly in their average BI (see METHODS; Fig. 3*D*). The overlap of all these measures is seen in the distribution of individual values superimposed on the histogram graphs of the mean values in Fig. 3, *A*, *C*, and *D*. Importantly, the distribution of soma sizes of GAD+ and GAD− neurons is largely overlapping. Soma size is the only feature that can be easily revealed by DIC microscopy and was used in many of the previous studies to indicate the identity of the recorded type of DCN neuron. Because of the overlap in the other measured morphological features, we concluded that randomly sampled GAD+ and GAD− neurons could not be differentiated unequivocally on morphological grounds only. Soma size becomes predictive for GAD− neurons only if the soma cross section is ≳300 μm^2 (soma diameter ≳25 μm).

Comparison of cell body areas (as measured from fixed samples stained for biocytin) with the corresponding apparent membrane capacitance (C_m; see METHODS) values obtained during electrophysiological whole cell recordings revealed that, as expected, larger cells had consistently larger C_m values (Fig. 3*E1*) but no such clear relationship was found between C_m and the maximal dendritic extension (Fig. 3*E2*). Therefore C_m can be taken as a reliable indicator of cell body size in cases where the cell morphology cannot be verified. The measured C_m values ranged from 33 to 271 pF (GAD− cells; average C_m 125 ± 9 pF) and 27 to 113 pF (GAD+ cells; average 56 ± 5 pF) and all cells with $C_m > 150$ pF had somata >300 μm^2.

Is it possible to identify GAD+ and GAD− cells on the basis of C_m values only? To answer this question we used the entire population of measured C_m values from pooled GAD− and GAD+ cells to fit a bimodal Gaussian curve constrained by the average C_m values from the two groups (Fig. 3*F*). The resulting probability curves suggest, in line with the above morphological observations, that (based on C_m values alone) only cells with $C_m > 150$ pF can be safely assumed to be GAD− cells. The majority of cells ($C_m < 150$), however, cannot be identified on the basis of their C_m value (or soma size). It should be mentioned that our sample did not include any of the "extremely small" GAD+ cells (soma length <10 μm, such as the one in Fig. 1*B*, in the *top* midarea of image).

Both GAD− and GAD+ cells are spontaneously active

DCN neurons in vivo typically fire spontaneously at 35–55 Hz (LeDoux et al. 1998; Rowland and Jaeger 2005; Thach 1968). During sensory stimulation or motor execution their firing frequency can reach hundreds of Hertz (e.g., Gruart et al. 2000). Also, they are known to fire APs spontaneously in vitro (slice preparation: Aizenman and Linden 1999; isolated cells: Raman et al. 2000).

We compared the rate of spontaneous firing of GAD+ and GAD− neurons with patch pipettes in the noninvasive cell-attached configuration (voltage-clamp mode). In both cell types, the frequency of spontaneous firing was not affected by blocking synaptic transmission with a cocktail of NBQX, AP5, and PiTX (data not shown). GAD− cells clearly fired faster (14.8 ± 2.1 Hz; $n = 13$) than did the GAD+ cells (9.9 ± 1.1 Hz, $n = 17$; pooled data from ACSF and synaptic blocker recordings; $P < 0.05$; Fig. 4, *A1–A3*). This difference was preserved (and even augmented) after breaking into whole cell configuration. Without injected bias current GAD− neurons fired at 29.9 ± 5.8 Hz ($n = 20$) and GAD+ neurons at 9.8 ± 1.0 Hz ($n = 19$; $P < 0.005$; experiments performed without synaptic blockers, Fig. 4, *B1–B3*).

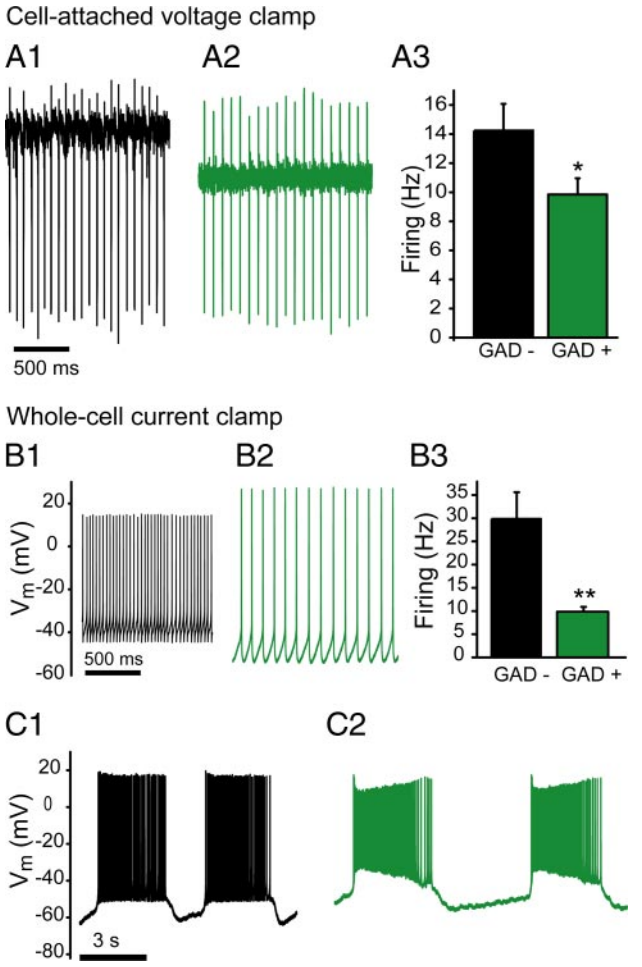

FIG. 4. Spontaneous firing of DCN neurons. *A1* and *A2*: example traces of cell-attached recordings form GAD− (*A1*) and GAD+ (*A2*) neurons. *A3*: bar graph of mean ± SE firing frequencies at 24°C. *B*: intracellularly recorded examples of spontaneous firing from GAD− (*B1*) and GAD+ (*B2*) cells at zero-bias current injection. *B3*: bar graph of the mean ± SE values. *C*: examples of spontaneous cyclic bursting activity observed in part of the GAD− (*C1*) and of GAD+ (*C2*) cells (*C1*, no current injection; *C2*, −3-pA current injection).

Spontaneous bursting, as previously described by Aizenman and Linden (1999), Czubayko et al. (2001), and others, was observed in both GAD− (20 of the 35 cells that had their bursting ability assessed by gradual hyperpolarization) and GAD+ cells (12 of 21 cells) (Fig. 4, *C1* and *C2*). The bursting GAD− cells tended to be larger in size (C_m on average 128 ± 10 vs. 84 ± 8 pF; $P < 0.05$) and have lower BI values than those of nonbursting ones (1.47 ± 0.09 vs. 2.31 ± 0.29; $P < 0.005$).

Action potential shapes of GAD+ and GAD− cells

For characterization of active and passive membrane properties, the DCN cells were current-clamped below but near to the threshold for spontaneous firing. We analyzed the shape of the first evoked AP (eAP) fired in response to series of depolarizing current steps of increasing amplitudes (0.3–1.8 pA/pF). To compare eAP shapes in GAD+ and GAD− cells, "grand average" eAP shapes (Fig. 5*A1*) were calculated as the average of all the average eAP shapes obtained from individual cells. These grand-average eAP shapes differed in several aspects between GAD+ and GAD− neurons. The most prominent difference between GAD− and GAD+ eAP shapes was their duration: GAD+ cells fired much broader eAPs than did the GAD− cells.

Even though the average eAP widths differed significantly (GAD−: 0.70 ± 0.05 ms, $n = 29$; GAD+: 0.99 ± 0.05 ms, $n = 22$; $P < 0.001$), the value ranges overlapped, as seen in the scatterplot in Fig. 5*A2* superimposed on the histogram of mean ± SE values. The GAD− cell eAP widths clustered into two groups with values above and below 0.6 ms, suggesting presence of more than one neuron population. In fact, plotting eAP width against cell capacitance (C_m; Fig. 5*B1*) and fitting the eAP width distri-

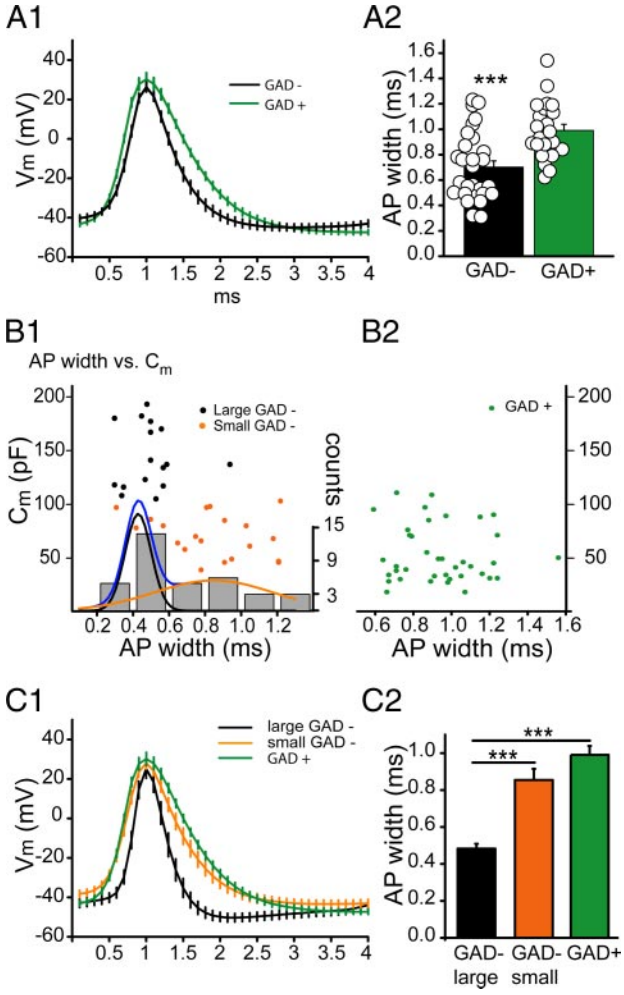

FIG. 5. Waveforms of evoked action potentials (APs). *A1*: peak-aligned grand averages of APs evoked by depolarizing current steps from subthreshold membrane potentials of GAD− and GAD+ cells. Vertical lines denote SE values. Note the significantly broader APs in GAD+ cells. *A2*: bar graph and distribution of individual AP widths. Bars are mean ± SE values; circles are individual values. *B1*: plot of C_m values against AP widths (dots) and a histogram of AP widths (gray bars). Blue line is a dual Gaussian fit (peaks at 0.43 ± 0.85 and 0.85 ± 0.23 ms) of AP width histogram; black and orange lines are the 2 Gaussian components of the fit. Individual values from large GAD− cells (C_m >100 pF) are plotted in black and those from small GAD− (C_m <100 pF) cells in orange. *B2*: C_m values of GAD+ neurons plotted vs. AP width. Note lack of correlation or clustering. *C1*: peak-aligned grand average AP waveforms from large and small GAD− cells and GAD+ cells. Vertical lines denote SE values. Note the similarity of small GAD− and GAD+ AP widths and the short-duration and fast afterhyperpolarization (AHP) of large GAD− cells. *C2*: bar graph of mean ± SE AP widths. ***$P < 0.001$.

bution with a bimodal Gaussian curve (with no constraints) reveals that large ($C_m \gtrsim 100$ pF; $n = 12$) GAD− neurons fire significantly shorter eAPs than small ($C_m < 100$ pF; $n = 17$) GAD-negative neurons (0.53 ± 0.03 vs. 0.85 ± 0.06 ms; $P < 0.001$). The corresponding plot for GAD+ cells did not reveal any correlation between eAP widths and C_m (Fig. 5*B2*). The GAD− cells were thus divided into two groups over this (somehow arbitrary) border value of 100 pF.

Even though the eAP induced by a step depolarization from a hyperpolarizing current keeping the voltage at subthreshold level is often used for quantification purposes in other cell types, in spontaneously firing neurons such as the DCN cells it does not reflect the natural situation. Thus we also analyzed AP shapes in steady-state firing cells using zero injected current (ssAPs, Fig. 6*A1*). As expected from the fact that tetrodotoxin (TTX)-sensitive sodium currents are partially inactivated at the interspike voltage ranges (Raman et al. 2000) ssAP widths were clearly broader in spontaneously active cells (large GAD−: 0.74 ± 0.07 ms, $n = 11$; small GAD−: 1.15 ± 0.18 ms, $n = 8$; GAD+: 1.48 ± 0.09 ms, $n = 12$) but large GAD− ssAP remained the fastest and GAD+ ssAPs the slowest (Fig. 6*A2*; ANOVA F = 14.85, $P < 0.0001$). In spontaneously firing cells the ssAP overshoots (peak amplitudes) of small GAD− and GAD+ neurons were significantly larger than those of large GAD− neurons (small GAD−: 27.1 ± 1.1 mV; GAD+: 21.0 ± 2.3 mV; large GAD−: 9.0 ± 4.4 mV; ANOVA F = 7.97, $P < 0.005$; Fig. 6*A3*), even though the membrane voltage from which the ssAP initiated did not differ significantly between cell groups (V_m at 2 ms before ssAP peak: large GAD−: −35.5 ± 2.0 mV; small GAD−: −33.1 ± 1.4 mV; GAD+: −38.6 ± 2.2 mV; ANOVA F = 1.83, $P = 0.178$).

Importantly, the three types of neurons differed in the expression of fast and slow AP afterhyperpolarizations (AHPs). GAD− cells (both large and small) exhibited a fast AHP (fAHP; Fig. 6, *B1* and *B2*), whereas both small GAD− and GAD+ neurons exhibited a pronounced slow AHP (sAHP; Fig. 6, *B2* and *B3*). There was no significant difference in the delay to fAHP peak in large and small GAD− cells (large GAD−: 4.05 ± 0.24 ms; small GAD−: 4.6 ± 0.3 ms; Fig. 6*C1*, *left*) or fAHP peak relative to V_m measured at 2 ms before peak (large GAD−: −9.1 ± 1.1 mV; small GAD−: −11.1 ± 2.1 mV; Fig. 6*C2*, *left*). The small GAD− and GAD+ cells did not differ in terms of the delay (from ssAP peak) before their sAHPs reached peaks (small GAD−: 31.0 ± 2.6 ms; GAD+: 34.7 ± 2.1 ms; $P = 0.3$; Fig. 6*C1*, *right*) but the GAD+ cells' sAHP amplitudes were significantly larger (−14.7 ± 0.9 mV) than those of the small GAD− (−11.7 ± 1.1 mV) or large GAD− (−9.5 ± 0.9 mV) cells (ANOVA F = 8.58, $P < 0.005$; Fig. 6*C2*, *right*). The AP and AHP parameters are summarized together with other electrophysiological measures in Table 2.

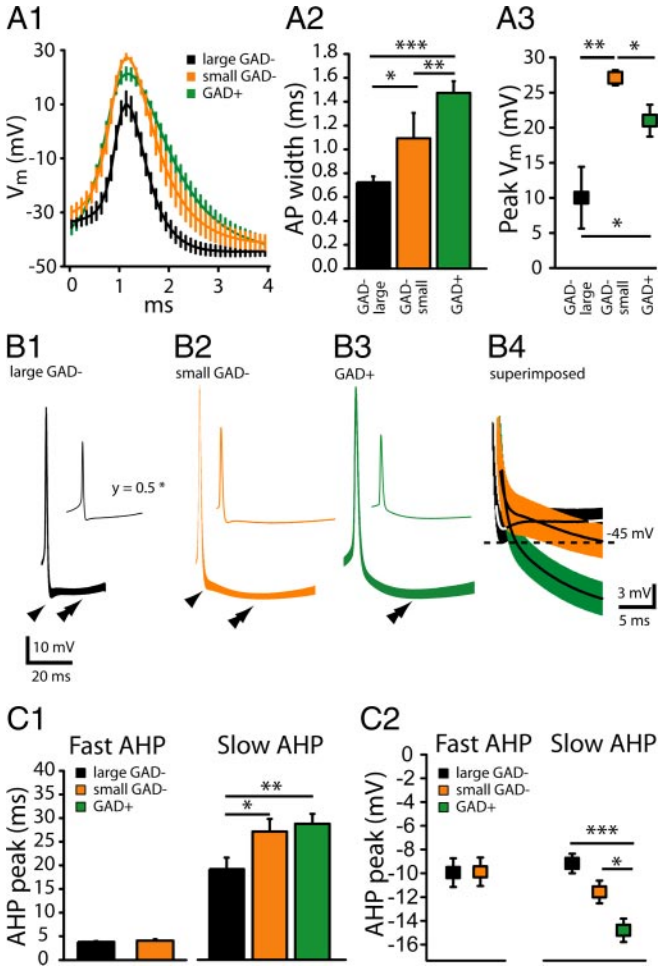

FIG. 6. Waveforms of spontaneously fired action potentials. *A1*: peak-aligned grand average of APs during steady-state firing (zero holding current) APs (ssAPs) of large and small GAD− cells and GAD+ cells. Vertical lines denote SE values. *A2* and *A3*: bar graph of mean ± SE ssAP widths (*A2*, measured at half-amplitude from 1 ms before AP peak) and box chart of ssAP peak amplitudes (*A3*), as mean ± SE values. Note the difference in AP widths between small GAD− and GAD+ cells, and larger amplitudes and peak values of small GAD− cells and GAD+ cells compared with large GAD− cells, even though the baseline is the same as (small GAD−) or more hyperpolarized (GAD+) than that in the large GAD− cells. *B1–B3*: grand average shapes of ssAPs at compressed timescale. Vertical width of trace indicates SE value. *Insets*: example traces of average ssAP shapes from individual cells. Note the presence of slow afterhyperpolarization (sAHP, double arrowheads in *B1–B3*) in all cells, but the absence of fast afterhyperpolarization (fAHP, single arrowheads in *B1* and *B2*) in GAD+ cells (*B3*). *B4*: peak-aligned, enlarged, and superimposed grand average ssAP shapes from large (black) and small (orange) GAD− and GAD+ (green) cells; the solid lines indicate mean value and width of colored area denotes SE. Note the differences in fAHP peak amplitude and timing. Horizontal dashed line indicates V_m value of −45 mV. *C1*: bar graph ± SE of average fAHP (*left*) and sAHP (*right*) peak times after the AP peak. *C2*: mean ± SE values of fAHP (*left*) and sAHP (*right*) peak voltages relative to V_m at 2 ms before AP peak. Asterisks denoting significant differences: $*P < 0.05$; $**P < 0.01$; $***P < 0.001$.

Dynamics of evoked AP firing in large and small GAD-negative cells and in GAD-positive cells

The dynamics of AP firing induced by injection of a current pulse is a classical criterion for classification of neuronal phenotypes. The firing frequency versus injected current (*f–I*) relationship provides information related to the sensitivity of a neuron to synaptic input. The adaptation of spike rate during a current pulse indicates how a neuron relays and integrates tonic (continuous) and phasic (burstlike) synaptic inputs. DCN neuron AP firing dynamics was studied using sets of depolarizing and hyperpolarizing current steps, normalized on the cell C_m (Fig. 7*A*). This normalization facilitates the comparison of cells of varying sizes (and thus input resistance). The *f–I* relationship of GAD+ cells was less steep than that of large and small GAD− cells (Fig. 7*B1*). Small GAD− cells had a sensitivity to injected current that did not differ from that of large GAD− cells at small current amplitudes but with larger currents their

TABLE 1. *Morphological parameters of DCN neurons*

Parameter	GAD−			GAD+		
	Mean	SE	*n*	Mean	SE	*n*
Soma area, μm^2	322	20	43	150	15	21
Soma length, μm	26	1.5	43	17	1.1	21
No. of primary dendrites	3.7	0.2	38	2.7	0.2	14
Branch index (BI)	1.88	0.14	37	1.44	0.08	13
Max. dendritic distance, μm	177	11	36	106	17	9

firing frequency saturated around 50 Hz. Notably, the ability to fire at high frequencies on depolarization was one of the most significant measures that differed between the large GAD− and the small GAD− and GAD+ cells.

Frequency adaptation during a 1-s depolarizing current step clearly differed between large GAD− and small GAD− and GAD+ cells. The large GAD− cells adapted on average only to roughly 80% of peak frequency, whereas the small GAD− and GAD+ cells slowed down to 50% of the peak frequency during the first 20 APs in a train where the average firing frequency was around 40 Hz (Fig. 7*B2*). Correspondent differences in frequency adaptations were also seen during the rebound depolarization (RD) on release from hyperpolarization (Fig. 7, *A1–A3*).

An I_h-like depolarizing sag during step hyperpolarization (Fig. 7*A*, single arrowheads) as well as RDs (Fig. 7*A*, double arrowheads) could be seen in all three of the cell groups studied. Even though the amount of I_h-like depolarization varied between cells of the same group (Fig. 7*C1*), no significant differences were found between the cell groups. In contrast, intriguing differences were observed in the duration of the RD (Fig. 7*C2*). Although there was no correlation between cell C_m and RD width (data not shown), the GAD+ cells exhibited much longer lasting RDs than did the GAD− cells, and the RDs in large GAD− cells were shorter than those in the small GAD− cells (GAD+: 1,728 ± 270 ms, $n = 16$; large GAD−: 638 ± 123 ms, $n = 8$; small GAD−: 936 ± 258, $n = 13$), although the cells were held at very similar V_m. Occasionally, the release from hyperpolarization triggered a very long-lasting "up-state" where cells continued to fire for many seconds before returning to the initial holding level; this property was most often seen in GAD+ cells. Almost all of these cells (five of six) also displayed spontaneous burst firing as shown in Fig. 4*C*.

Temperature dependency of the AP firing properties

To compare our results with those obtained in vivo or at higher experimental temperatures, we investigated the effect of recording temperature on the key electrophysiological parameters. We analyzed five large GAD−, four small GAD−, and nine GAD+ cells that were recorded first at 24°C followed by a switch to 34°C. The effects of temperature on the AP shape parameters and firing characteristics are exemplified in Fig. 8. With raising the temperature from 24 to 34°C, the eAP half-widths decreased from 0.65 ± 0.07, 1.23 ± 0.15, and 1.14 ± 0.08 to 0.38 ± 0.03, 0.79 ± 0.12, and 0.77 ± 0.08 (large GAD−, small GAD−, and GAD+ cells, respectively) (Fig. 8*A1*). The ssAP half-widths decreased (large GAD−, small GAD−, and GAD+ cells, respectively) from 0.93 ± 0.05, 1.39 ± 0.17, and 1.63 ± 0.14 to 0.56 ± 0.09, 0.82 ± 0.1, and 1.01 ± 0.09 (Fig. 8*A2*). The shortening of eAP and ssAP half-width in these cells was used to calculate the Q10 values as follows: Q10 for eAP: large GAD−, 1.84 ± 0.05; small GAD−, 1.73 ± 0.14; GAD+, 1.87 ± 0.07; Q10 for ssAP: large GAD−, 2.07 ± 0.26; small GAD−, 1.84 ± 0.04;

TABLE 2. *Electrophysiological parameters of DCN neurons at room temperature*

	Large GAD−			Small GAD−			GAD+		
	Mean	SE	*n*	Mean	SE	*n*	Mean	SE	*n*
Input resistance, MΩ	220	22	18	572	69	18	1,069	91	24
Membrane time constant (tau), ms	33.1	4.3	18	36.8	3.7	18	55.7	6.2	24
C_m, pF	141.7	7.4	18	69.2	4.3	18	55.9	5.4	24
Spontaneous firing frequency (external recording), Hz	16.9	1.9	9	8.3	2.2	4	9.8	1.1	16
Spontaneous firing frequency (whole cell), Hz	30.6	5.8	13	28.5	13.2	7	9.9	1.0	19
eAP peak V_m, mV	27.5	4.1	12	28.0	11.4	17	30.2	3.3	22
eAP half-width, ms	0.53	0.03	12	0.85	0.06	17	0.99	0.05	22
ssAP threshold V_m, mV	−35.5	2.0	11	−33.1	1.4	8	−38.6	2.2	12
ssAP peak V_m, mV	10.0	2.3	11	27.1	1.1	8	21.0	2.3	12
ssAP half-width, ms	0.74	0.07	11	1.15	0.18	8	1.52	0.09	12
ssAP fAHP peak time, ms	4.05	0.24	11	4.6	0.30	6	NA	NA	NA
ssAP fAHP peak V_m (relative to prespike V_m), mV	−9.1	1.1	11	−11.1	2.1	6	NA	NA	NA
ssAP sAHP peak time, ms	19.19	2.43	8	31.0	2.6	7	34.7	2.1	12
ssAP sAHP peak V_m, mV	−9.5	0.9	9	−11.7	1.06	7	−14.7	0.9	12

C_m, apparent cell capacitance; eAP, evoked action potential, ssAP, steady-state action potential; fAHP, fast afterhyperpolarization; sAHP, slow afterhyperpolarization. NA, data not available.

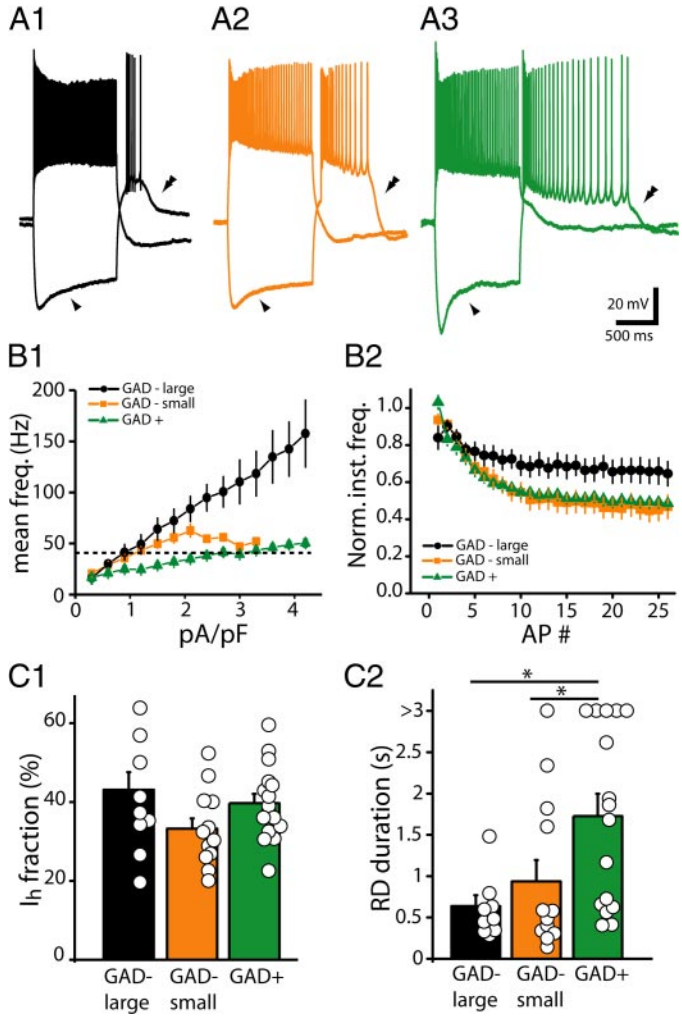

FIG. 7. Action potential firing dynamics. *A*: example traces of firing dynamics of large (*A1*) and small (*A2*) GAD− and GAD+ (*A3*) DCN neurons. Voltage responses evoked by 1-s, ±1.5-pA/pF current steps from subthreshold holding membrane potentials. Strong frequency adaptation in small GAD− and GAD+ cells can be seen both in response to depolarizing current step and during the rebound depolarization (RD, double arrowheads). Note the presence and qualitative similarity of hyperpolarizing current (I_h)–like voltage sags (single arrowheads) and RD after release from hyperpolarization in all cell types. *B*: quantification of AP firing dynamics. *B1*: firing vs. injected current (*f–I*) plot. Steeper slope of GAD− cells compared with GAD+ cells shows that the GAD− cells are more sensitive to input strength than the GAD+ cells. Note firing frequency saturation of small GAD− neurons around 50 Hz. Horizontal dashed line marks 40-Hz mean firing frequency, which was used in quantification of firing accommodation (*B2*). *B2*: frequency adaptation during depolarizing current step inducing a nearly 40-Hz mean firing rate. Instantaneous firing frequency (1/interspike interval) was normalized for the maximal value in each cell and the mean values are plotted against the AP number in the AP train. Vertical lines denote SE values. Note that the GAD+ (green) and small GAD− (orange) cells display a more pronounced frequency accommodation than the large GAD− (black) cells. *C1*: quantification of I_h-like currents in terms of the depolarizing sag in response to hyperpolarizing current pulse (−1.5 pA/pF). Differences between cell groups are not significant. *C2*: quantification of the RD duration at half-amplitude. Bar graph (mean ± SE) and individual data points: $^*P < 0.05$.

GAD+, 1.79 ± 0.08. The averaged temperature dependency of AP half-width in DCN can be given as a Q10 value of 1.86 ± 0.05.

The spontaneous firing frequency (recorded with no bias current injection) increased in all cells [from 19.8 ± 5.1, 3.9 ± 0.4, and 7.34 ± 1.23 Hz to 34.2 ± 7.0, 12.0 ± 0 ($n = 1$), and 14.4 ± 2.8 Hz, large GAD−, small GAD−, and GAD+ cells, respectively] but the firing accommodation or bursting behavior did not change qualitatively. As an example of this, Fig. 8*B* shows two RDs triggered by a release from hyperpolarization in a large GAD− and a GAD+ cell; note the similar firing pattern at both temperatures.

DISCUSSION

In the present study, we morphologically and electrophysiologically characterized three neuronal populations of the DCN: the GABAergic neurons and large and small non-GABAergic neurons. GAD67 has been widely used as a marker in studies requiring identification of GABAergic cells in different brain areas including the DCN (e.g., Molineux et al. 2006). In contrast to transgenic mice in which an ectopic GAD67 promoter drives expression of a fluorescent marker protein, GFP was targeted to the locus encoding GAD67 using a homologous recombination in the GAD67-GFP knock-in mice used in the present study (Tamamaki et al. 2003). Although this method ensures, to the best of our understanding, a faithful expression of GFP in GAD67-expressing cells, it is accompanied by the potential caveat that reduced GAD67 activity in heterocygotous knock-in mice causes an alteration of the cellular parameters studied here. We have no reason, however, to believe that such alterations occur. As for the identity of the GAD− neurons, it is reasonable to assume that the majority of these cells are glutamatergic (Chen and Hillman 1993). Because we did not demonstrate the transmitter content of these cells, we simply refer to them collectively as "non-GABAergic cells." We cannot exclude the possibility that the cells categorized here as "small GAD-negative cells" would be GABAergic and lack (for any unknown reason) GFP fluorescence; however, our results demonstrate that their properties differed significantly from the GAD+ cells (and "large GAD− cells") in several parameters.

Another issue requiring note is the division of GAD-negative cells into large and small neurons. As is evident from Fig. 5*B1*, the large and small GAD-negative cells overlap in terms of AP width and thus the cells with $C_m \approx 100$ pF cannot clearly be allocated to either type based on the C_m value alone. In general, we found that the identification of individual DCN neurons based on their electrophysiological properties requires a combination of several measures. The electrophysiological dynamics of large non-GABAergic cells enables them to faithfully relay tonic spike rate information, whereas small non-GABAergic and GABAergic neurons are specialized for relaying and integrating phasic input.

Morphological characteristics of DCN neurons

It has been well established that DCN neurons have complex and diverse morphologies. Correlating biocytin-label–based cell morphometry with the transmitter genotype did not reveal dendritic branching patterns that would be indicative for the neurotransmitter content. On average, the GABAergic neurons have smaller cell bodies and less complex dendritic arborization so that GABAergic cells can be described as "scaled-down" versions of the non-GABAergic (likely glutamatergic) cells.

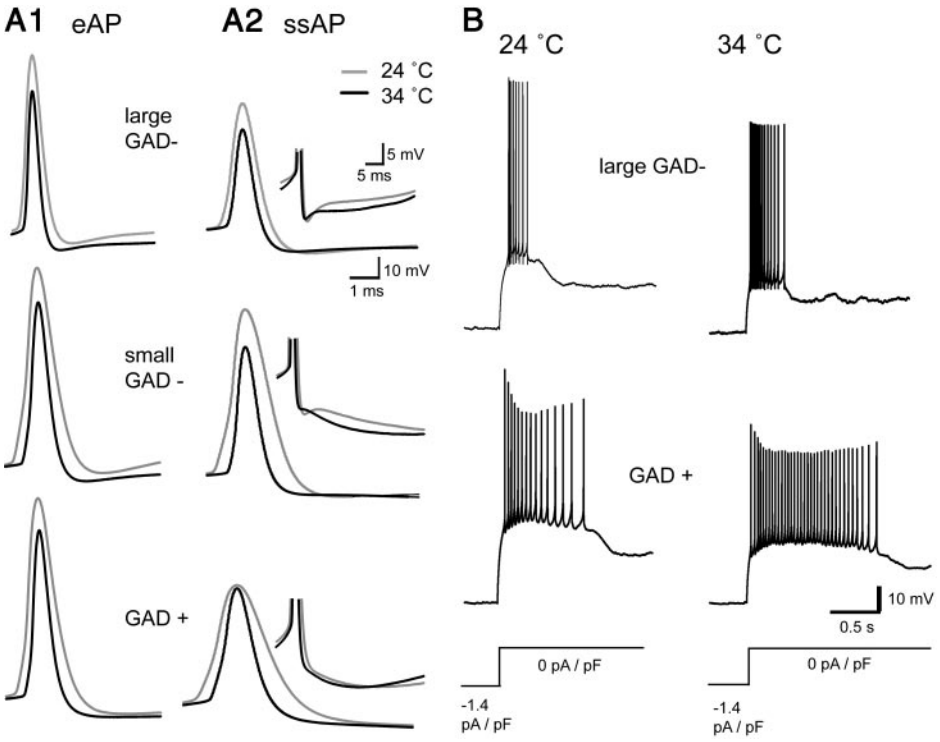

FIG. 8. Effect of temperature on action potential firing in DCN cells. *A*: example traces of evoked action potentials (eAPs, *A1*) and steady-state action potentials (ssAPs, *A2*) from individual large GAD−, small GAD− and GAD+ cells in room temperature (gray line) and physiological temperature (black line), aligned on the AP peak and AP threshold. *Inset* in *A2* shows in compressed timescale the presence of fAHPs in GAD− cells and their absence in GAD+ cells, even at higher temperature. *B*: example traces from large GAD− (*top*) and a GAD+ (*bottom*) cells showing the RD response to release from a −1.4-pA/pF hyperpolarizing current step in room temperature (*left*) and physiological temperature (*right*). Note that the general properties of the RD do not change, even though the firing frequency and RD duration can increase.

Dendritic spines (Aizenman et al. 2003) were seen in all cell types. We saw cell morphologies corresponding to all of the types originally described by Chan-Palay (1977) except for the smallest ("6," small bridging neurons), which we did not target. All cells with clearly columnar dendritic organization (resembling Chan-Palay's "large columnar cells") recovered were GAD-negative. As a result of the lower success rate in patching small (soma length <15 μm) cells, our sample is biased toward somewhat larger cells.

Spontaneous activity of GABAergic and non-GABAergic DCN neurons

DCN neurons have been known to spontaneously fire APs at several tens of Hertz in vivo and (in the absence of synaptic transmission) in vitro. Our present work demonstrates that both GABAergic and non-GABAergic DCN neurons are intrinsically active. Interestingly, and in contrast to the cell types described in many cortical structures, both large and small GAD-negative cells fire slightly (but significantly) faster than the GABAergic cells (Fig. 4). Under the premise that spontaneous firing of DCN neurons is promoted by resurgent sodium current (Raman et al. 2000) our data suggest that this current is expressed in all cell types included in the study.

We could induce burst firing, as described in earlier studies both in vitro (Aizenman and Linden 1999; Czubayko et al. 2001) and in vivo (Rowland and Jaeger 2005), in all cell types. Thus the expression of bursting activity is not indicative for the neurotransmitter used by the cell, consistent with a concurrent study by Molineux and colleagues (2006). An earlier compartmental modeling study of medioventral vestibular nucleus neurons (that share many properties with DCN neurons) demonstrated that the ability to generate burst firing critically depends on the number of primary dendrites (Quadroni and Knöpfel 1994). This number varies largely within each group of the DCN neurons (Figs. 2 and 3) and thus could be the determinant of bursting likelihood. Statistical confirmation of this hypothesis was not possible with the available number of cells with completely recovered biocytin-labeled dendritic trees.

Action potential waveforms of GABAergic and non-GABAergic DCN neurons

APs evoked by depolarizing steps from subthreshold holding voltages were much faster in non-GABAergic than in GABAergic DCN neurons (Fig. 5). This, again, contrasts to neuron categories described in the cerebral cortex where GABAergic neurons are often characterized by faster APs (Jonas et al. 2004; Swadlow 2003). The distribution of AP widths of non-GABAergic neurons was broad and this measure along with the cell capacitance suggested that these neurons could be divided into two groups that we termed large and small GAD-negative (GAD−) cells (Fig. 5). The distinction between these two groups of GAD-negative DCN neurons was further supported by observed differences in AP afterpotentials and spike train dynamics (see following text).

Induction of APs from subthreshold holding potentials recruits ionic currents that are partially inactivated or deactivated during normal spontaneous firing of DCN neurons. Therefore we also characterized the AP waveforms during spontaneous steady-state activity. Not surprisingly, steady-state APs in all cell types were broader than the evoked APs. However, the relative differences in AP widths observed between the subgroups with evoked APs remained and were even more pronounced under steady-state conditions (Fig. 6).

Finally, the three groups of DCN neurons differed in the expression of fast and slow spike AHPs. During steady-state spontaneous firing conditions, all large GAD− and almost all small GAD− cells underwent a fast afterhyperpolarization

(fAHP) in <5 ms after the AP peak, whereas all GAD+ cells hyperpolarized slower, reaching their AHP peaks only about 25 ms after the AP peak. The GAD− cells often underwent a second, slower AHP (sAHP) after the fAHP that peaked with similar delays after AP peak as the GAD+ cells.

A complete biophysical explanation of the difference in AP width and AHP waveform is beyond the scope of the present study. However, it could be speculated that the differences are due to distinct expression patterns of Kv3 potassium channel subtypes that are known to affect AP duration and amplitude and that are expressed at high levels in the DCN (Goldman-Wohl et al. 1994; McMahon et al. 2004). In addition, the diversity in AHP shapes may be related to differential expression of large-conductance (BK) and small-conductance (SK) potassium currents (Sausbier et al. 2004; Shakkottai et al. 2004). Generation of the fAHP likely involves longitudinal currents between soma and dendrites (Quadroni and Knöpfel 1994) and extensive damage of dendrites during slicing can thus result in lack of clear fAHPs. This may explain why in two of nine small GAD− cells a fAHP was not clearly seen. The slow AHP is mediated, at least in part, by SK channels (Shakkottai et al. 2004) and our results suggest a higher expression level of these channels in GABAergic than in non-GABAergic DCN neurons.

Spike rate dynamics

The three populations of DCN neurons had different dynamics of AP firing evoked by a depolarizing step. Large GAD− neurons were characterized by a steep frequency-to-current (*f–I*) relationship and little frequency adaptation. The small GAD− cells initially increased their firing rate similarly but leveled off at a lower maximal frequency. GABAergic neurons had a shallow *f–I* relationship and exhibited, like small GAD− neurons, significant frequency adaptation. The steep *f–I* relation endows the large GAD− cells to faithfully relay spike frequency information. The shallow slope of the *f–I* relationship along with frequency adaptation and pronounced rebound excitation in GABAergic cells points toward a function in processing phasic spike frequency information. Thus timing of GABAergic cell activity may carry information that is more relevant than the average firing frequency. Interestingly, our results on the differences in *f–I* relationship and frequency adaptation fit well with predictions from modeling studies (Benda and Herz 2003; Engel et al. 1999) that implicate stronger expression of SK-type calcium-activated potassium channels in cells with spike rate dynamics of the type observed in GABAergic DCN neurons.

In agreement with the suggestion that the RD is mainly triggered by T-type Ca^{2+}-channels (Aizenman and Linden 1999; Jahnsen 1986; Llinas and Muhlethaler 1988; Molineux et al. 2006; Muri and Knöpfel 1994; Raman et al. 2000), there was no correlation between the strength of RD and I_h (as shown in Fig. 7*C1*).

Electrophysiological identification of DCN neurons

Our results define criteria for reliable identification of living GABAergic and non-GABAergic DCN neurons without the need of morphological measures or genetic labeling. Identification of large GAD− cells is straightforward and partly compatible with the earlier concepts of identifying "large cells" as glutamatergic. Combining the analysis of C_m distribution (Fig. 3*F*) and AP width distribution (Fig. 5*A2*) indicates that cells with C_m >125 pF and AP widths <0.6 ms belong to the large GAD− neurons (in our sample only one of ten GAD− cells with C_m >125 pF had AP width >0.6 ms). For cells with C_m <125 pF the most reliable identifying criterion was the presence of a fAHP during steady-state firing (in our sample, none of the 21 cells with C_m <125 pF and expressing a clear fAHP was GAD+). However, the mere absence of a clear fAHP does not prove that the cell is GABAergic: in two of nine small GAD− cells the fAHP was not clearly seen.

GABAergic cells can be reliably identified by C_m <50 pF, lack of a fAHP, and the presence of sAHP with amplitude > −15 mV [measured as the difference between the V_m at 2 ms before peak AP and minimal V_m during sAHP (15 to 40 ms after AP peak)].

Functional implications and future directions

The presence of GABAergic cells in the DCN has been known for decades (Chan-Palay 1977; Houser et al. 1984). However, most models of the function of the cerebellar circuitry treat the DCN as a simple relay station whose throughput is under inhibitory control of Purkinje cells and has little computational significance (e.g., Medina and Mauk 2000). However, Purkinje neurons can inhibit GABAergic DCN neurons and thereby disinhibit glutamatergic projection neurons. Furthermore, frequency adaptation and rebound excitation between the three groups of DCN neurons enrich the dynamics of the DCN circuit with time constants in the range of several milliseconds to seconds that may be relevant for computation of motor command dynamics (Lisberger and Sejnowski 1992). It is thus important to note that the GABAergic and the small cells exhibited more frequency adaptation and stronger rebound excitation than did the large GAD− cells. Large GAD− cells, conversely, act more like linear transducers of spike rate information as often assumed in cerebellar network models (Medina et al. 2001; Ohyama et al. 2002). A complete picture of the signal processing within the DCN requires additional data on cell-type–specific projection patterns, intrinsic connectivity, and synaptic dynamics. The present data provide a framework for advances along these lines.

ACKNOWLEDGMENTS

We thank Y. Iwamoto, N. Horiguchi, and N. Saitoh for expert help in animal handling, genotyping, and digital imaging and all members of the Knöpfel Lab for many helpful discussions.

GRANTS

This work was supported by an intramural grant from the RIKEN Brain Science Institute.

REFERENCES

Afshari FS, Ptak K, Khaliq ZM, Grieco TM, Slater NT, McCrimmon DR, Raman IM. Resurgent Na currents in four classes of neurons of the cerebellum. *J Neurophysiol* 92: 2831–2843, 2004.

Aizenman CD, Huang EJ, Linden DJ. Morphological correlates of intrinsic electrical excitability in neurons of the deep cerebellar nuclei. *J Neurophysiol* 89: 1738–1747, 2003.

Aizenman CD, Linden DJ. Regulation of the rebound depolarization and spontaneous firing patterns of deep nuclear neurons in slices of rat cerebellum. *J Neurophysiol* 82: 1697–1709, 1999.

Bäurle J, Grüsser-Cornehls U. Differential number of glycine- and GABA-immunopositive neurons and terminals in the deep cerebellar nuclei of normal and Purkinje cell degeneration mutant mice. *J Comp Neurol* 382: 443–458, 1997.

Benda J, Herz AV. A universal model for spike-frequency adaptation. *Neural Comput* 15: 2523–2564, 2003.

Chan-Palay V. *Cerebellar Dentate Nucleus: Organization, Cytology and Transmitters.* Heidelberg, Germany: Springer-Verlag, 1997.

Chen S, Hillman DE. Colocalization of neurotransmitters in the deep cerebellar nuclei. *J Neurocytol* 22: 81–91, 1993.

Czubayko U, Sultan F, Their P, Schwarz C. Two types of neurons in the rat cerebellar nuclei as distinguished by membrane potentials and intracellular fillings. *J Neurophysiol* 85: 2017–2029, 2001.

De Zeeuw CI, Berrebi AS. Postsynaptic targets of Purkinje cell terminals in the cerebellar and vestibular nuclei of the rat. *Eur J Neurosci* 7: 2322–2333, 1995.

Engel J, Schultens HA, Schild D. Small conductance potassium channels cause an activity-dependent spike frequency adaptation and make the transfer function of neurons logarithmic. *Biophys J* 76: 1310–1319, 1999.

Fredette BJ, Mugnaini E. The GABAergic cerebello-olivary projection in the rat. *Anat Embryol (Berl)* 184: 225–243, 1991.

Goldman-Wohl DS, Chan E, Baird D, Heintz N. Kv3.3b: a novel Shaw type potassium channel expressed in terminally differentiated cerebellar Purkinje cells and deep cerebellar nuclei. *J Neurosci* 14: 511–522, 1994.

Gruart A, Guillazo-Blanch G, Fernandez-Mas R, Jimenez-Diaz L, Delgado-Garcia JM. Cerebellar posterior interpositus nucleus as an enhancer of classically conditioned eyelid responses in alert cats. *J Neurophysiol* 84: 2680–2690, 2000.

Houser CR, Barber RP, Vaughn JE. Immunocytochemical localization of glutamic acid decarboxylase in the dorsal lateral vestibular nucleus: evidence for an intrinsic and extrinsic GABAergic innervation. *Neurosci Lett* 47: 213–220, 1984.

Jahnsen H. Extracellular activation and membrane conductances of neurones in the guinea-pig deep cerebellar nuclei in vitro. *J Physiol* 372: 149–168, 1986.

Jonas P, Bischofberger J, Fricker D, Miles R. Interneuron diversity series: fast in, fast out–temporal and spatial signal processing in hippocampal interneurons. *Trends Neurosci* 27: 30–40, 2004.

LeDoux MS, Hurst DC, Lorden JF. Single-unit activity of cerebellar nuclear cells in the awake genetically dystonic rat. *Neuroscience* 86: 533–545, 1998.

Lisberger SG, Sejnowski TJ. Motor learning in a recurrent network model based on the vestibulo-ocular reflex. *Nature* 360: 159–161, 1992.

Llinas R, Muhlethaler M. Electrophysiology of guinea-pig cerebellar nuclear cells in the in vitro brain stem-cerebellar preparation. *J Physiol* 404: 241–258, 1988.

McMahon A, Fowler SC, Perney TM, Akemann W, Knöpfel T, Joho RH. Allele-dependent changes of olivocerebellar circuit properties in the absence of the voltage-gated potassium channels Kv3.1 and Kv3.3. *Eur J Neurosci* 19: 3317–3327, 2004.

Medina JF, Garcia KS, Mauk MD. A mechanism for savings in the cerebellum. *J Neurosci* 21: 4081–4089, 2001.

Medina JF, Mauk MD. Computer simulation of cerebellar information processing. *Nat Neurosci Suppl* 3: 1205–1211, 2000.

Molineux ML, McRory JE, McKay BE, Hamid J, Mehaffey WH, Rehak R, Snutch TP, Zamponi GW, Turner RW. Specific T-type calcium channel isoforms are associated with distinct burst phenotypes in deep cerebellar nuclear neurons. *Eur J Neurosci* 24: 2581–2594, 2006.

Muri R, Knöpfel T. Activity induced elevations of intracellular calcium concentration in neurons of the deep cerebellar nuclei. *J Neurophysiol* 71: 420–428, 1994.

Ohyama T, Medina JF, Nores WL, Mauk MD. Trying to understand the cerebellum well enough to build one. *Ann NY Acad Sci* 978: 425–438, 2002.

Quadroni R, Knöpfel T. Compartmental models of type A and type B guinea pig medial vestibular neurons. *J Neurophysiol* 72: 1911–1924, 1994.

Raman IM, Gustafson AE, Padgett D. Ionic currents and spontaneous firing in neurons isolated from the cerebellar nuclei. *J Neurosci* 20: 9004–9016, 2000.

Rowland NC, Jaeger D. Coding of tactile response properties in the rat deep cerebellar nuclei. *J Neurophysiol* 94: 1236–1251, 2005.

Sausbier M, Hu H, Arntz C, Feil S, Kamm S, Adelsberger H, Sausbier U, Sailer CA, Feil R, Hofmann F, Korth M, Shipston MJ, Knaus HG, Wolfer DP, Pedroarena CM, Storm JF, Ruth P. Cerebellar ataxia and Purkinje cell dysfunction caused by Ca^{2+}-activated K^+ channel deficiency. *Proc Natl Acad Sci USA* 101: 9474–9478, 2004.

Shakkottai VG, Chou CH, Oddo S, Sailer CA, Knaus HG, Gutman GA, Barish ME, LaFerla FM, Chandy KG. Enhanced neuronal excitability in the absence of neurodegeneration induces cerebellar ataxia. *J Clin Invest* 113: 582–590, 2004.

Silberberg G, Grillner S, LeBeau FE, Maex R, Markram H. Synaptic pathways in neural microcircuits. *Trends Neurosci* 28: 541–551, 2005.

Sultan F, Czubayko U, Thier P. Morphological classification of the rat lateral cerebellar nuclear neurons by principal component analysis. *J Comp Neurol* 455: 139–155, 2003.

Swadlow HA. Fast-spike interneurons and feedforward inhibition in awake sensory neocortex. *Cereb Cortex* 13: 25–32, 2003.

Tamamaki N, Yanagawa Y, Tomioka R, Miyazaki J, Obata K, Kaneko T. Green fluorescent protein expression and colocalization with calretinin, parvalbumin, and somatostatin in the GAD67-GFP knock-in mouse. *J Comp Neurol* 467: 60–79, 2003.

Teune TM, van der Burg J, De Zeeuw CI, Voogd J, Ruigrok TJ. Single Purkinje cell can innervate multiple classes of projection neurons in the cerebellar nuclei of the rat: a light microscopic and ultrastructural triple-tracer study in the rat. *J Comp Neurol* 392: 164–178, 1998.

Thach WT. Discharge of Purkinje and cerebellar nuclear neurons during rapidly alternating arm movements in the monkey. *J Neurophysiol* 31: 785–797, 1968.